

Quantum thermoelectric diodes and transistors with squeezed reservoir engineering

Ziming Wang(王子明), Gaoyuan Chen(陈高远), Yongkang Liu(刘永康), Chenhui Yu(俞晨晖), Yue Wu(吴越), Zi Wang(王子), Hongzhao Sun(孙红照), and Jincheng Lu(陆金成)

Citation: Chin. Phys. B, 2026, 35 (**4**): 040502. DOI: 10.1088/1674-1056/ae2abb
http://cpb.iphy.ac.cn; http://iopscience.iop.org/cpb

What follows is a list of articles you may be interested in

Phase transition of interfacial water at low-dimensions

Wenlong Liang(梁文龙), Yujie Huang(黄雨婕), Yue Zhang(张悦), and Chunlei Wang(王春雷)
Chin. Phys. B, 2026, 35 (**2**): 020501. DOI: 10.1088/1674-1056/ae12da

Thermodynamics of classical one-dimensional generalized nonlinear Klein-Gordon lattice model

Hu-Wei Jia(贾虎伟) and Ning-Hua Tong(同宁华)
Chin. Phys. B, 2025, 34 (**8**): 080501. DOI: 10.1088/1674-1056/add50f

Resonant tunneling diode cellular neural network with memristor coupling and its application in police forensic digital image protection

Fei Yu(余飞), Dan Su(苏丹), Shaoqi He(何邵祁), Yiya Wu(吴亦雅), Shankou Zhang(张善扣), and Huige Yin(尹挥戈)
Chin. Phys. B, 2025, 34 (**5**): 050502. DOI: 10.1088/1674-1056/adb8bb

Two innovative equivalent statements of the third law of thermodynamics

Xiaohang Chen(陈晓航), Yinghui Zhou(周颖慧), and Jincan Chen(陈金灿)|
Chin. Phys. B, 2024, 33 (**6**): 060504. DOI: 10.1088/1674-1056/ad39c8

Effects of notch structures on DC and RF performances of AlGaN/GaN high electron mobility transistors

Hao Zou(邹浩), Lin-An Yang(杨林安), Xiao-Hua Ma(马晓华), and Yue Hao(郝跃)
Chin. Phys. B, 2021, 30 (**4**): 040502. DOI: 10.1088/1674-1056/abd470

Quantum thermoelectric diodes and transistors with squeezed reservoir engineering

Ziming Wang(王子明)[1,2], Gaoyuan Chen(陈高远)[1,2], Yongkang Liu(刘永康)[1,2], Chenhui Yu(俞晨晖)[1,2], Yue Wu(吴越)[3], Zi Wang(王子)[4,†], Hongzhao Sun(孙红照)[1,2,‡], and Jincheng Lu(陆金成)[1,2,§]

[1] *Key Laboratory of Intelligent Optoelectronic Devices and Chips of Jiangsu Higher Education Institutions, School of Physical Science and Technology, Suzhou University of Science and Technology, Suzhou* 215009, *China*

[2] *Advanced Technology Research Institute of Taihu Photon Center, School of Physical Science and Technology, Suzhou University of Science and Technology, Suzhou* 215009, *China*

[3] *Suzhou Wujiang District Xinsheng Experimental School, Suzhou* 215009, *China*

[4] *Department of Physics, National University of Singapore, Singapore* 117551, *Singapore*

(Received 13 September 2025; revised manuscript received 4 December 2025; accepted manuscript online 10 December 2025)

This work investigates inelastic thermoelectric systems exhibiting tight relations among electronic charge, electronic heat, and photonic heat currents. By employing a double quantum dot setup interacting with a squeezed photon reservoir, we show that such architectures can operate as high-performance quantum thermoelectric diodes and transistors. Central to this capability is the role of quantum squeezing, which markedly enhances the rectification of both charge and heat currents. Moreover, we demonstrate that a photon-assisted inelastic transport mechanism sustains a thermal transistor effect even within the linear-response regime — a regime where conventional elastic devices typically fail to amplify heat currents. Notably, quantum squeezing further enhances the thermal gain, underscoring its utility in quantum heat control. These results not only deepen our understanding of nonequilibrium quantum thermoelectrics but also provide a viable pathway toward designing devices with tailored energy-conversion functionalities through quantum reservoir engineering.

Keywords: thermoelectrics, quantum thermodynamics, diode, transistors

PACS: 05.70.–a, 72.20.Pa, 85.30.–z, 05.60.Gg

DOI: 10.1088/1674-1056/ae2abb **CSTR:** 32038.14.CPB.ae2abb

1. Introduction

Photon-mediated thermoelectric systems remain a vibrant frontier in condensed matter physics, marrying fundamental scientific inquiry with prospects for energy harvesting and thermal management.[1,2] This interdisciplinary domain connects mesoscopic transport with open quantum dynamics, fueling advances not only in energy conversion[3,4] but also in hybrid quantum systems such as quantum-dot circuit QED.[5,6] Recent explorations of quantum dots subjected to simultaneous voltage and thermal biases have unveiled profound influences of quantum squeezing on both electronic and bosonic transport, suggesting new mechanisms for quantum-enhanced thermoelectric performance.[7,8] As a versatile resource for controlling fluctuations and correlations in nonequilibrium settings, squeezing has emerged as a key tool for probing quantum thermodynamics and designing functional devices.[9,10] Despite these developments, the realization of coherent photon–thermoelectric devices — especially those exhibiting diode-like and transistor-like behaviors — continues to pose a significant challenge, driving ongoing experimental and theoretical efforts.

Among various nonclassical resources,[11] squeezed thermal reservoirs stand out for their exceptional ability to enhance performance in quantum thermal devices.[12–17] By redistributing thermal fluctuations between conjugate variables, squeezing enables phase-controlled work extraction beyond classical limits, improves energy conversion efficiency via correlated electron–photon exchange, and allows simultaneous optimization of power and efficiency, which is unattainable in conventional thermal systems. In particular, quantum squeezing serves as a key resource for enhancing interference-based energy transfer and enabling noise-resilient operation. These quantum effects can be significantly amplified through tailored squeezing parameters, highlighting the potential of squeezed photonic environments in practical thermoelectric applications.

In this work, we investigate photon-assisted inelastic thermoelectric transport in a double quantum dot system coupled to a squeezed photon reservoir. We demonstrate that quantum squeezing serves as a potent tool for the coherent control of thermoelectric performance, enabling enhanced manipulation of charge and energy currents. By combining a quantum master equation approach with full counting statistics, we reveal that electron–photon interactions introduce essential non-

†Corresponding author. E-mail: wangzi@nus.edu.sg

‡Corresponding author. E-mail: sunhongzhao@usts.edu.cn

§Corresponding author. E-mail: jinchenglu@usts.edu.cn

© 2026 Chinese Physical Society and IOP Publishing Ltd. All rights, including for text and data mining, AI training, and similar technologies, are reserved.

linearities into the transport characteristics. When synergized with squeezing-induced phase coherence, these nonlinearities allow strong rectification of both charge and heat currents through gate tuning of the quantum dot energy levels. Moreover, we show that a three-terminal configuration sustains a thermal transistor effect within the linear-response regime, and quantum squeezing can further enhance the thermal gain. Our results establish squeezed photon reservoirs as a versatile platform for achieving unprecedented quantum control over mesoscopic thermoelectric energy conversion. Throughout this work, we adopt natural units with $\hbar = k_{\rm B} = e = 1$ for simplicity.

2. The model and methods

We consider a three-terminal setup, composed of a double quantum dot system inelastically coupled to a squeezed photon bath. Each dot individually exchanges energy with an electronic reservoir (e.g., metal lead, denoted as l and r), as shown in Fig. 1. The Hamiltonian of the whole system reads[2]

$$\hat{H} = \hat{H}_{\rm DQD} + \hat{H}_{\text{e-ph}} + \hat{H}_{\rm lead} + \hat{H}_{\rm tun} + \hat{H}_{\rm ph}, \tag{1}$$

with the constituent terms defined as

$$\hat{H}_{\rm DQD} = \sum_{i={\rm l,r}} \varepsilon_i \hat{d}_i^\dagger \hat{d}_i + t(\hat{d}_{\rm l}^\dagger \hat{d}_{\rm r} + {\rm H.c.}), \tag{2a}$$

$$\hat{H}_{\rm ph} = \sum_q \omega_q \hat{a}_q^\dagger \hat{a}_q, \tag{2b}$$

$$\hat{H}_{\text{e-ph}} = \sum_q \gamma_{\text{e-ph}} (\hat{d}_{\rm l}^\dagger \hat{d}_{\rm r} + \hat{d}_{\rm r}^\dagger \hat{d}_{\rm l})(\hat{a}_q + \hat{a}_q^\dagger), \tag{2c}$$

$$\hat{H}_{\rm lead} = \sum_{j={\rm l,r}} \sum_k \varepsilon_{jk} \hat{d}_{jk}^\dagger \hat{d}_{jk}, \tag{2d}$$

$$\hat{H}_{\rm tun} = \sum_{v={\rm l,r};k} \gamma_{vk} \hat{d}_v^\dagger \hat{d}_{vk} + {\rm H.c.} \tag{2e}$$

Here, $\hat{d}_i^\dagger$ ($\hat{d}_i$) is the creation (annihilation) operator for an electron on the i-th quantum dot, ε_i is the on-site energy, and t is the inter-dot tunneling amplitude. $\hat{H}_{\rm ph}$ describes the squeezed photon bath, where $\hat{a}_q^\dagger$ ($\hat{a}_q$) is the creation (annihilation) operator for a photon with frequency ω_q. The inelastic electron–photon interaction is captured by $\hat{H}_{\text{e-ph}}$, with a coupling strength $\gamma_{\text{e-ph}}$. $\hat{H}_{\rm lead}$ represents the electronic reservoirs, and $\hat{H}_{\rm tun}$ describes the tunneling between the quantum dots and their respective leads, with γ_{vk} denoting the tunneling coupling strength.

We begin by considering a multimode bosonic field described by the Hamiltonian $\hat{H}_{\rm ph}$. This field is in a squeezed thermal state if its density matrix takes the form[18]

$$\rho_{\rm ph} = \hat{S}(z)\rho_{\rm th}\hat{S}^\dagger(z), \tag{3}$$

where $\rho_{\rm th} = {\rm e}^{-\beta\hat{H}_{\rm ph}}/Z$ is the thermal state and $\hat{S}(z) = {\rm e}^{\sum_q (z^* \hat{a}_q^2 + z\hat{a}_q^{\dagger 2})}$, where $z = r{\rm e}^{{\rm i}\theta_q}$ is the squeezing parameter, $r \geq 0$ is the squeezing amplitude and θ_q is the squeezing angle. This operator applies Bogoliubov transformations to the photonic operators $\sum_q \hat{S}(z)\hat{a}_q\hat{S}^\dagger(z) = \sum_q \hat{a}_q \cosh(r) + {\rm e}^{{\rm i}\theta_q}\hat{a}_q^\dagger \sinh(r)$. Using these transformations, the expectation values for the second moments in the state (3) are found to be

$$\langle \hat{a}_q^\dagger \hat{a}_q \rangle = (n_{\rm ph} + 1/2)\cosh(2r) - 1/2, \tag{4a}$$

$$\langle \hat{a}_q \hat{a}_q \rangle = (n_{\rm ph} + 1/2){\rm e}^{{\rm i}\theta_q}\sinh(2r). \tag{4b}$$

Here $n_{\rm ph} = 1/({\rm e}^{\beta_{\rm ph}\omega_q} - 1)$ is the Bose–Einstein distribution.

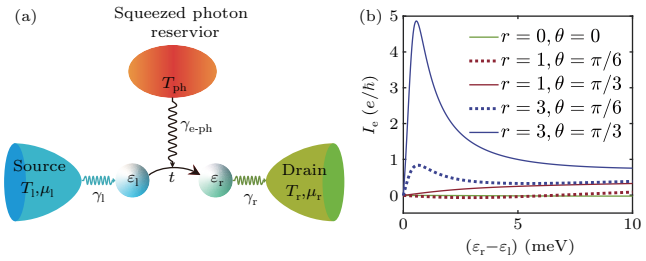


Fig. 1. (a) Illustration of the three-terminal inelastic thermoelectric device. An electron leaves the source into the left QD with energy $\varepsilon_{\rm l}$ and hops to the right QD with a different energy $\varepsilon_{\rm r}$ assisted by a photon from the photon reservoir (with temperature $T_{\rm ph}$). The temperatures and chemical potentials of the two electronic reservoirs are $T_{\rm l(r)}$ and $\mu_{\rm l(r)}$, respectively. The temperature of the photon reservoir is $T_{\rm ph}$. t is the tunneling between the two QDs, $\gamma_{\rm l}$ ($\gamma_{\rm r}$) is the coupling between the dots and the left (right) reservoir, and $\gamma_{\text{e-ph}}$ is the strength of the electron–photon interaction. (b) The charge current $I_{\rm e}$ as a function of level detuning $\varepsilon_{\rm r} - \varepsilon_{\rm l}$. The other parameters are given by $\mu = 0$ meV, $\Delta\mu = 2$ meV, $\varepsilon_{\rm l} = 0$, $\Gamma_{\rm l} = \Gamma_{\rm r} = \Gamma_{\rm ph} = 4$ meV, $t = 8$ meV, and $k_{\rm B}T_{\rm l} = k_{\rm B}T_{\rm r} = k_{\rm B}T_{\rm ph} = 10$ meV.

Separately, we diagonalize the double quantum dot Hamiltonian, $\hat{H}_{\rm DQD}$, by introducing new electronic operators via the transformation[19] $\hat{d}_{\rm l} = \cos\alpha\hat{d} - \sin\alpha\hat{D}$ and $\hat{d}_{\rm r} = \sin\alpha\hat{d} + \cos\alpha\hat{D}$,[19] with $\alpha \equiv \frac{1}{2}\arctan\left(\frac{2t}{\varepsilon_{\rm r}-\varepsilon_{\rm l}}\right)$. The corresponding energy levels are given by $\varepsilon_D = \frac{\varepsilon_{\rm r}+\varepsilon_{\rm l}}{2} + \sqrt{\frac{(\varepsilon_{\rm r}-\varepsilon_{\rm l})^2}{4} + t^2}$ and $\varepsilon_d = \frac{\varepsilon_{\rm r}+\varepsilon_{\rm l}}{2} - \sqrt{\frac{(\varepsilon_{\rm r}-\varepsilon_{\rm l})^2}{4} + t^2}$.

Based on the two-time measurement protocol,[20] we apply full counting statistics to obtain the particle and energy flows out of the electronic reservoirs and the heat current out of the photon reservoir by including $\chi = \{\lambda_{\rm p}, \lambda_E, \lambda_{\rm ph}\}$, respectively. Consequently (see Appendix A), the counting-field-dependent total Hamiltonian is described as $\hat{H}_{-\chi/2} = \hat{H}_{\rm DQD} + \hat{H}_{\rm ph} + \hat{H}_{\rm lead} + \hat{H}_I^{-\chi/2}$, with $\hat{H}_I^{-\chi/2}$ specified as

$$\begin{aligned}\hat{H}_I^{-\chi/2} = &\sum_q \gamma_{\text{e-ph}} \Big[\sin(2\alpha)(\hat{D}^\dagger\hat{D} - \hat{d}^\dagger\hat{d}) \\ &+ \cos(2\alpha)(\hat{d}^\dagger\hat{D} + \hat{D}^\dagger\hat{d})\Big]({\rm e}^{{\rm i}\frac{\lambda_{\rm ph}}{2}\omega_q}\hat{a}_q + {\rm H.c.}) \\ &+ \sum_k \Big(\Big[\gamma_{rk}(\sin\alpha\hat{D}^\dagger + \cos\alpha\hat{d}^\dagger)\hat{d}_{rk} \\ &+ \gamma_{lk}{\rm e}^{{\rm i}\frac{\lambda_{\rm p}}{2} + {\rm i}\frac{\lambda_E}{2}\varepsilon_{lk}}(\cos\alpha\hat{D}^\dagger - \sin\alpha\hat{d}^\dagger)\hat{d}_{lk}\Big] + {\rm H.c.}\Big).\end{aligned} \tag{5}$$

We assume the electron–photon coupling and dot-reservoir tunnelings are weak. Based on the Born–Markov approximation, we perturb $H_I^{-\chi/2}$ to obtain the quantum master

equation as[21]

$$\frac{\partial}{\partial t}\rho_{\rm S}(\chi,t) = {\rm i}[\rho_{\rm S}(\chi,t), H_{\rm DQD}] - \int_0^\infty {\rm d}\tau {\rm Tr}_{\rm B}\{[[\hat{H}_{-\chi/2}, [\hat{H}_{-\chi/2}(-\tau), \rho_{\rm S}(\chi,t)\otimes\rho_{\rm B}]_\chi]_\chi\}, \quad (6)$$

where $\rho_{\rm S}(\chi,t)$ denotes the reduced density operator of the central double QD system with counting parameters, i.e., $\rho_{\rm S}(\chi,t) = {\rm Tr}_{\rm B}\{\rho_\chi^{\rm T}(t)\}$, with $\rho_\chi^{\rm T}(t)$ the full density operator of the whole inelastic heat engine. The commutation relation denotes $[\hat{A}_\chi, \hat{B}_\chi]_\chi = \hat{A}_\chi\hat{B}_\chi - \hat{B}_\chi\hat{A}_{-\chi}$, and the equilibrium distribution of reservoirs is specified as $\rho_{\rm B} = \rho_{\rm l}\otimes\rho_{\rm r}\otimes\rho_{\rm ph}$, with $\rho_i = \exp\left[-\beta_i(\hat{H}_i - \mu_i\hat{N}_i)\right]/Z_i$ $(i = {\rm l},{\rm r})$, the partition functions $Z_i = {\rm Tr}\left\{\exp\left[-\beta_i(\hat{H}_i - \mu_i\hat{N}_i)\right]\right\}$, and the inverse temperatures $\beta_i = 1/k_{\rm B}T_i$. $\rho_{\rm ph}$ is the density matrix of the squeezed photon bath defined in Eq. (3). The explicit form of the quantum master equation with full counting statistics is shown in Appendix B.

Computing the transport for this model within the quantum master equation formalism requires knowledge of the eigenproblem of the double quantum dot system $H_{\rm DQD}$. The electronic basis is $|0\rangle$, $|d\rangle$, $|D\rangle$, and the vector made of the populations and coherences of $\rho_{\rm S}(\chi,t)$ in this basis is denoted by $\dot{\rho}_{mn} = \langle m|\rho_{\rm S}|n\rangle$, with $m,n = 0,d,D,Dd$. If we reorganize $\rho_{\rm S}(\chi,t)$ in vector form $|\boldsymbol{P}(\chi,t)\rangle\rangle = [\langle m|\rho_{\rm S}(\chi,t)|n\rangle]$ $(m = 0,D,d,Dd)$, the quantum master equation is reexpressed as

$$\frac{{\rm d}|\boldsymbol{P}(\chi,t)\rangle\rangle}{{\rm d}t} = \boldsymbol{L}(\chi)|\boldsymbol{P}(\chi,t)\rangle\rangle, \quad (7)$$

where $\boldsymbol{L}(\chi)$ is the evolution matrix with its elements shown in Appendix B. These elements are tightly related to the dissipation strengths $\Gamma_\nu(\varepsilon) \equiv 2\pi\sum_k |t_{k\nu}|^2\delta(\varepsilon - \varepsilon_k)$ $(\nu = {\rm l},{\rm r})$ and $\Gamma_{\rm ph}(\omega) \equiv 2\pi\sum_q |\lambda_q|^2\delta(\omega - \omega_q)$. In the following, we set these dissipation strengths as constant for convenience without losing generality.

After long-time evolution, the cumulant generating function based on the large deviation principle is $\mathcal{G}(\chi) = E_{\rm g}(\chi)$. Here $E_{\rm g}(\chi)$ corresponds to the eigenvalue of $\boldsymbol{L}(\chi)$ with the largest real part, characterizing the dominant mode of the system dynamics. Consequently, the current flowing from the left reservoir into the system is given by[22,23]

$$I_\nu(t) = \frac{\partial\mathcal{G}(\chi)}{\partial({\rm i}\lambda_\nu)}\Big|_{\chi=0}, \quad (8)$$

where $\nu = e,E,{\rm ph}$. Meanwhile, the electronic heat flow extracted from the left reservoir is defined as $I_Q^{\rm l} = I_E^{\rm l} - \mu_{\rm l}I_{\rm e}^{\rm l}$.[24] In analogy, the particle current $I_{\rm e}^{\rm r}$ and energy current $I_E^{\rm r}$ flow from the right electronic reservoir into the central system. Particle conservation implies $I_{\rm e}^{\rm l} + I_{\rm e}^{\rm r} = 0$, and energy conservation requires $I_E^{\rm l} + I_E^{\rm r} + I_Q^{\rm ph} = 0$.[25]

We define the net charge current and net heat current as[3,26]

$$I_{\rm e} \equiv \frac{1}{2}(I_{\rm e}^{\rm r} - I_{\rm e}^{\rm l}), \quad I_Q^{\rm e} \equiv \frac{1}{2}(I_Q^{\rm r} - I_Q^{\rm l}), \quad (9)$$

respectively.

Before delving into a detailed discussion, it is essential to note that the methods employed in this study rely on the assumption of weak system-reservoir couplings, denoted as γ_i $(i = {\rm l},{\rm r},{\rm ph})$. In our previous work, we demonstrated that quantum coherence effects can enhance the energy conversion efficiency of quantum heat engines,[27] as well as induce rectification and thermal transistor effects.[28] Here, we further show that squeezing is also a significant quantum effect. However, it is important to emphasize that squeezing and coherence effects coexist, because the squeezing parameters r and θ only manifest in the off-diagonal elements of the density matrix–specifically, in the terms $\langle D|\rho_{\rm S}|d\rangle$ and $\langle d|\rho_{\rm S}|D\rangle$, which correspond to elements $H_{4i(i4)}$ and $H_{5i(i5)}$ of the evolution matrix.

In Fig. 1(b), with a fixed chemical potential difference of $\Delta\mu = 2$ meV, we show the net charge current $I_{\rm e}$ as a function of the QD energy difference $\varepsilon_{\rm r} - \varepsilon_{\rm l}$ for different values of the squeezing amplitude r and squeezing angle θ. It is evident that larger values of r and θ lead to a significant enhancement of the charge current.

3. Rectification effects

In this section, we illustrate that the three-terminal configuration effectively behaves as a diode.[29–36] Our system, renowned for its combined thermal and electrical transport capabilities, offers the potential for unconventional rectification effects. Notably, it can induce charge rectification owing to a temperature difference, in addition to the conventional charge rectification driven by a voltage bias.[26,37]

In a general nonequilibrium setup, the charge rectification effects can be characterized as

$$R_{\rm e} = \frac{|I_{\rm e}(\Delta\mu) + I_{\rm e}(-\Delta\mu)|}{|I_{\rm e}(\Delta\mu)| + |I_{\rm e}(-\Delta\mu)|}, \quad (10)$$

which is induced by the chemical potential. The thermal rectification induced by a temperature gradient is defined as

$$R_{\rm t} = \frac{|I_Q^{\rm e}(\Delta T) + I_Q^{\rm e}(-\Delta T)|}{|I_Q^{\rm e}(\Delta T)| + |I_Q^{\rm e}(-\Delta T)|}. \quad (11)$$

The rectification coefficients $R_{\rm e}$ and $R_{\rm t}$ quantify the degree of asymmetry in the charge and heat currents when the applied bias (chemical potential difference $\Delta\mu$ or temperature difference ΔT) is reversed. Both coefficients are bounded between 0 and 1. A value of $R = 0$ indicates perfect symmetry, i.e., $I(\Delta) = -I(-\Delta)$, implying no rectification. As R approaches 1, the current under forward bias becomes

much larger than under reverse bias, signaling strong rectification. These definitions are standard in the analysis of thermal and electronic diodes and provide a convenient dimensionless measure of device performance.

Here, we demonstrate pronounced charge and heat rectification effects in a three-terminal quantum dot device coupled to a squeezed photon reservoir, as illustrated in Fig. 2. In the purely elastic transport regime ($\Gamma_{\rm ph} = 0$), both charge and heat currents exhibit nearly symmetric behavior with respect to bias reversal, as shown in Figs. 2(a) and 2(b). While a finite inelastic coupling ($\Gamma_{\rm ph} \neq 0$) generally introduces some asymmetry even for fixed dot energies (as visible, for instance, in the brown curve of Fig. 1(b)), a pronounced and tunable rectification effect emerges decisively when the inelastic scattering is combined with a suitable detuning of the quantum dot energy levels, as demonstrated in Figs. 2(c)–2(f). This confirms that inelastic scattering, when synergized with gate-tunable level positions, serves as a fundamental and controllable mechanism for achieving strong rectification.[26]

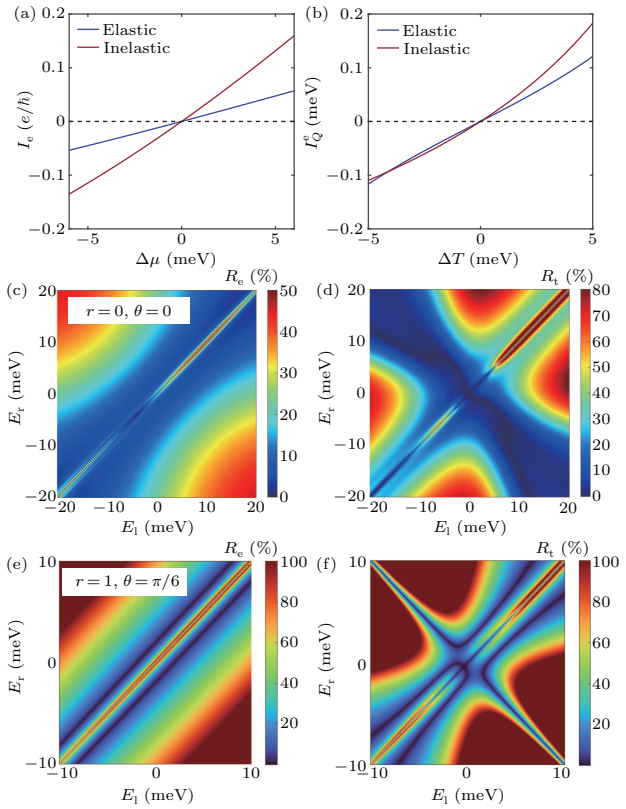


Fig. 2. Charge and heat-rectification effects. (a) Charge current I_e as a function of $\Delta\mu$, (b) the heat current I_Q^e as a function of ΔT for different $\Gamma_{\rm ph}$, where $\varepsilon_l = 5$ meV and $\varepsilon_r = 7$ meV. (c) The charge rectification R_e and (e) the heat rectification R_t as functions of quantum dot energies ε_l and ε_r without squeezing effects, where $r = 0$ and $\theta = 0$. (d) The charge rectification R_e and (f) the heat rectification R_t as functions of quantum dot energies ε_l and ε_r with squeezing effects, where $r = 1$ and $\theta = \pi/6$. The other parameters are given by $\Gamma_l = \Gamma_r = \Gamma_{\rm ph} = 4$ meV, $t = 4$ meV, and $k_B T_l = k_B T_r = 10$ meV.

We further investigate the role of quantum squeezing — controlled via the amplitude r and phase θ — in enhancing rectification performance. By systematically tuning the quantum dot energy levels ε_l and ε_r, we compare rectification behavior both in the presence and absence of squeezing. As evidenced in Figs. 2(c)–2(f), the rectification ratios for both charge (R_e) and heat (R_t) are substantially amplified under squeezing conditions. This enhancement can be attributed to the squeezing-induced modification of photon statistics and the corresponding amplification of coherence-assisted transport channels. These results clearly indicate that quantum squeezing not only elevates the magnitude of charge and heat currents but also profoundly enhances their asymmetric character under bias reversal. We therefore conclude that the synergy between inelastic scattering and squeezed photon states provides a powerful mechanism for controlling thermal and electrical rectification at the nanoscale.

The dependence of the rectification coefficients on the squeezing parameters is summarized in Fig. 3. For charge rectification R_e (panel (a)), the coefficient increases monotonically with the squeezing amplitude r, whereas its variation with the squeezing angle θ is more subtle and non-monotonic, generally decreasing as θ increases from 0 to π under the chosen parameters. In contrast, the thermal rectification R_t (panel (b)) exhibits a pronounced enhancement with both r and θ, growing significantly as θ increases. Notably, due to the 2π-periodicity of the current with respect to θ, both R_e and R_t display mirror symmetry around $\theta = \pi$. Overall, these results clearly demonstrate that quantum squeezing can substantially enhance rectification effects, providing a versatile means to tailor charge and heat transport asymmetries through the control of squeezing amplitude and phase.

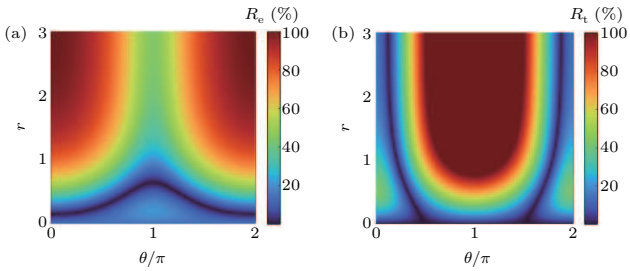


Fig. 3. (a) The charge rectification R_e for $\Delta\mu = 10$ meV and $\Delta T = 0$, and (b) the heat rectification R_t as functions of the squeezing amplitude r and angle θ for $\Delta\mu = 0$ and $\Delta T = 15$ meV, where $r = 0$ and $\theta = 0$. The other parameters are given by $\varepsilon_l = -5$ meV and $\varepsilon_r = 5$ meV, $\Gamma_l = \Gamma_r = \Gamma_{\rm ph} = 4$ meV, $t = 4$ meV, $\mu = 4$ meV, and $k_B T_l = k_B T_r = 10$ meV.

4. Thermal transistor effects in the linear-response regime

The heat amplification effect, where a small change in the base current significantly alters the collector-emitter current, enables quantum thermal transistors for precise energy control, see Figs. 4(a) and 4(b). While traditionally believed to require nonlinear transport and negative differential thermal conductance,[38,39] recent studies have shown that thermal transistor effects can also occur in the linear-response

regime under photon-assisted inelastic transport.[26] Our previous work demonstrated such effects in circuit QED systems across a broad range of quantum dot energies and light-matter couplings,[37] and even in Brownian thermal transistors without these conditions, using Gaussian fluctuation theory.[40] However, all existing studies remain confined to the canonical thermal reservoir regime,[28,41–44] and the role of quantum squeezed effects in thermal transistors remains an open question.

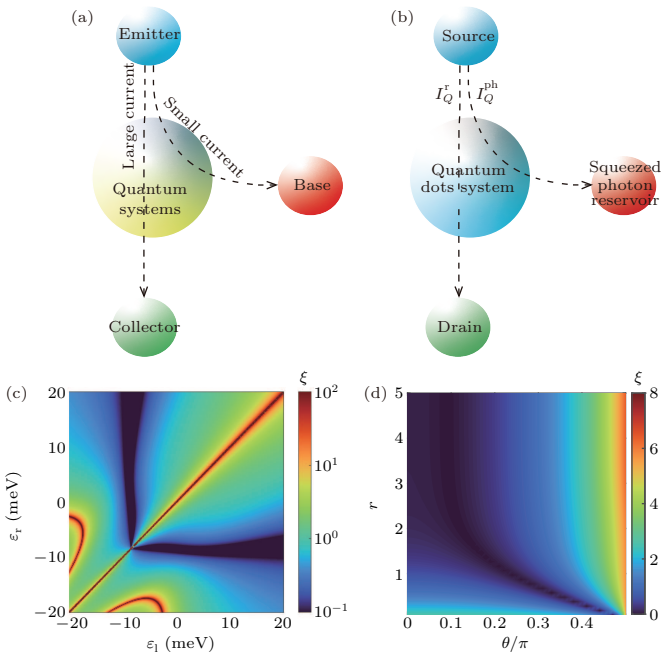


Fig. 4. (a) In a conventional transistor, a small base-emitter charge current controls a much larger emitter-collector charge current, with their ratio defining the transistor effect. (b) In a three-terminal quantum-dot based photon-thermoelectric transistor, a small heat current from the source to the photon reservoir ($I_Q^{\rm ph}$) modulates a larger heat current from source to drain ($I_Q^{\rm r}$). The ratio of these currents, denoted as the heat amplification factor ξ, characterizes the thermal transistor effect. (c) ξ as a function of QD energies $\varepsilon_{\rm l}$ and $\varepsilon_{\rm r}$ with $r=1$ and $\theta=\pi/2$. (d) ξ as a function of r and θ with $\varepsilon_{\rm l}=9$ meV and $\varepsilon_{\rm r}=10$ meV. The other parameters are given by $\Gamma_{\rm l}=\Gamma_{\rm r}=\Gamma_{\rm ph}=4$ meV, $t=4$ meV, $\mu=4$ meV, $k_{\rm B}T_{\rm l}=k_{\rm B}T_{\rm r}=10$ meV.

In the purely thermal conduction scenario ($\Delta\mu=0$), the system's linear thermal transport is captured by[42,45]

$$\begin{pmatrix} I_Q^{\rm r} \\ I_Q^{\rm ph} \end{pmatrix} = \begin{pmatrix} K_{rr} & K_{rp} \\ K_{rp} & K_{pp} \end{pmatrix} \begin{pmatrix} T_{\rm r}-T_{\rm l} \\ T_{\rm ph}-T_{\rm l} \end{pmatrix}, \tag{12}$$

where K_{ij} denote the linear-response thermal conductances. A key quantity characterizing the thermal transistor effect is the heat amplification factor, defined as

$$\xi = \left| \frac{\partial_{T_{\rm ph}} I_Q^{\rm r}}{\partial_{T_{\rm ph}} I_Q^{\rm ph}} \right| = \frac{K_{rp}}{K_{pp}}. \tag{13}$$

As illustrated in Figs. 4(c) and 4(d), the amplification factor ξ can exceed unity in the linear-response regime due to inelastic photon-assisted transport. It exhibits strong sensitivity to the quantum dot energies $\varepsilon_{\rm l}$ and $\varepsilon_{\rm r}$, which are tunable via gate voltages. Owing to system symmetry, ξ varies symmetrically with respect to these energy levels. Thermal amplification occurs within specific parameter ranges, for example when $\varepsilon_{\rm l}<-5$ meV and $\varepsilon_{\rm r}<-10$ meV, or when both $\varepsilon_{\rm l}$ and $\varepsilon_{\rm r}$ are positive, under squeezed reservoir conditions with $r=1$ and $\theta=\pi/2$. Notably, ξ diverges when $\varepsilon_{\rm r}=\varepsilon_{\rm l}$, consistent with the Fermi golden rule expression $\alpha=|\varepsilon_{\rm l}/(\varepsilon_{\rm r}-\varepsilon_{\rm l})|$ for weak electron–photon coupling.[26]

We further examine the impact of squeezing parameters on the amplification. Figure 4(d) shows that $\xi>1$ for $\theta\gtrsim 0.3\pi$, while variations in the squeezing amplitude r have a comparatively weaker influence. These results indicate that quantum squeezing can enhance the thermal transistor effect, although its role in the linear-response regime is more subtle than in rectification phenomena.

5. Conclusion

In summary, we have demonstrated the potential of inelastic thermoelectric systems as functional quantum devices–including diodes and transistors–by exploiting photon-mediated electron transport. A central finding is that squeezed photon reservoirs provide tunable quantum control over transport properties. By engineering the quantum dot energy profiles, we achieve strong rectification in both charge and heat currents, which is further enhanced through squeezing-induced coherence. Additionally, a three-terminal architecture supports thermal transistor operation even in the linear-response regime, with inelastic processes enabling heat amplification. Squeezing modifies the amplification factor and extends its dynamic range, highlighting the capacity of quantum photonic environments to surpass classical limits in thermoelectric energy conversion and enabling coherent control of quantum thermal devices.

Appendix A: Full counting statistics for particle, energy, and photonic currents

We employ the framework of full counting statistics (FCS) to fully characterize the fluctuations of particle and energy currents in our three-terminal quantum system. This approach allows us to compute not only the average currents flowing into each reservoir ($\nu={\rm l,r,ph}$) but also their higher-order cumulants and correlations. Following the standard two-time measurement protocol, we define the characteristic (moment generating) function as the central quantity for statistical analysis.

The characteristic function is given by

$$\mathcal{Z}(\chi) = \left\langle \mathrm{e}^{\mathrm{i}\sum_\mu \lambda_\mu \hat{Q}_\mu(0)}\, \mathrm{e}^{-\mathrm{i}\sum_\mu \lambda_\mu \hat{Q}_\mu(t)} \right\rangle, \tag{A1}$$

where $\chi=\{\lambda_{\rm p},\lambda_E,\lambda_{\rm ph}\}$ denotes the set of counting fields conjugate to the extensive observables

$$\hat{Q}_\mu \equiv \{\hat{N}_{\rm r},\hat{H}_{\rm r},\hat{H}_{\rm ph}\}, \tag{A2}$$

which correspond to the particle number in the right electronic reservoir, the electronic energy in the right reservoir, and the photonic energy in the photon reservoir, respectively.

The initial state of the total system is assumed to factorize as

$$\rho_T(0) = \rho_{\rm S}(0) \otimes \rho_{\rm l}(0) \otimes \rho_{\rm r}(0) \otimes \rho_{\rm ph}(0), \tag{A3}$$

where each reservoir state $\rho_\alpha(0)$ is described by a thermal equilibrium distribution. This factorization is essential for deriving a tractable expression for the generating function.

Equivalently, the characteristic function can be expressed through the modified density operator as

$$\mathcal{Z}(\chi,t) = {\rm Tr}\Big[\rho_\chi^{\rm T}(t)\Big], \tag{A4}$$

with

$$\rho_\chi^{\rm T}(t) = {\rm e}^{-{\rm i}H_{-\chi/2}t}\,\rho_T(0)\,{\rm e}^{{\rm i}H_{\chi/2}t}, \tag{A5}$$

where the counting-field-dependent Hamiltonians are defined by the canonical transformation

$$H_{\pm\chi/2} = {\rm e}^{\mp{\rm i}\sum_\mu \lambda_\mu \hat{Q}_\mu/2} H_T\, {\rm e}^{\pm{\rm i}\sum_\mu \lambda_\mu \hat{Q}_\mu/2}. \tag{A6}$$

This transformation effectively incorporates the measurement protocol into the system evolution.

The cumulant generating function (CGF) is then obtained as

$$\mathcal{G}(\chi) = \lim_{t\to\infty} \frac{1}{t} \ln \mathcal{Z}(\chi), \tag{A7}$$

which encodes all cumulants of the current distributions. In particular, the first-order cumulants yield the average currents:

$$I_\mu = \frac{\partial \mathcal{G}(\chi)}{\partial({\rm i}\lambda_\mu)}\Big|_{\chi=0}, \tag{A8}$$

where $\mu = {\rm p}, E, {\rm ph}$ denotes the particle, electronic energy, and photonic energy currents, respectively. Higher-order derivatives with respect to the counting fields give access to current noise and higher-order statistical moments.

This FCS formalism is particularly suited for quantum-coherent systems, as it captures both the average transport behavior and the fluctuations, which are crucial for understanding the fundamental limits of nanoscale energy conversion and the thermodynamic performance of quantum heat engines.

Appendix B: Quantum master equation and Liouvillian operator elements

In this appendix, we provide the explicit expression of the quantum master equation (QME) including full counting statistics (FCS) as derived from Eq. (6). After performing the standard Born-Markov and secular approximations and neglecting high-frequency rotating terms, the QME in the Schrödinger picture reads

$$\frac{\partial}{\partial t}\rho_{\rm S}(\chi,t) = -{\rm i}[\hat{H}_{\rm DQD},\rho_{\rm S}] + \mathcal{L}_{\rm l}[\rho_{\rm S}] + \mathcal{L}_{\rm r}[\rho_{\rm S}] + \mathcal{L}_{\rm ph}[\rho_{\rm S}], \tag{B1}$$

where each Liouvillian superoperator $\mathcal{L}_v$ for $v = {\rm l},{\rm r},{\rm ph}$ is given by

$$\begin{aligned}\mathcal{L}_{\rm l}[\rho_{\rm S}] \;=\; & \Gamma_{\rm l}\sin^2\alpha\, f_{\rm l}(\varepsilon_D)\Big({\rm e}^{+{\rm i}\lambda_{\rm p}+{\rm i}\lambda_E\varepsilon_D}\hat{D}^\dagger\rho_{\rm S}\hat{D} - \frac{1}{2}\{\rho_{\rm S},\hat{D}\hat{D}^\dagger\}\Big) + \Gamma_{\rm l}\sin^2\alpha\,[1-f_{\rm l}(\varepsilon_D)]\Big({\rm e}^{-{\rm i}\lambda_{\rm p}-{\rm i}\lambda_E\varepsilon_D}\hat{D}\rho_{\rm S}\hat{D}^\dagger - \frac{1}{2}\{\rho_{\rm S},\hat{D}^\dagger\hat{D}\}\Big)\\ & + \Gamma_{\rm l}\cos^2\alpha\, f_{\rm l}(\varepsilon_d)\Big({\rm e}^{+{\rm i}\lambda_{\rm p}+{\rm i}\lambda_E\varepsilon_d}\hat{d}^\dagger\rho_{\rm S}\hat{d} - \frac{1}{2}\{\rho_{\rm S},\hat{d}\hat{d}^\dagger\}\Big) + \Gamma_{\rm l}\cos^2\alpha\,[1-f_{\rm l}(\varepsilon_d)]\Big({\rm e}^{-{\rm i}\lambda_{\rm p}-{\rm i}\lambda_E\varepsilon_d}\hat{d}\rho_{\rm S}\hat{d}^\dagger - \frac{1}{2}\{\rho_{\rm S},\hat{d}^\dagger\hat{d}\}\Big)\\ & + \text{cross terms proportional to } \sin\alpha\cos\alpha,\end{aligned} \tag{B2}$$

coupling between $\hat{D}$ and $\hat{d}$ with appropriate Fermi factors and counting fields.

$$\begin{aligned}\mathcal{L}_{\rm r}[\rho_{\rm S}] \;=\; & \Gamma_{\rm r}\cos^2\alpha\, f_{\rm r}(\varepsilon_D)\Big(\hat{D}^\dagger\rho_{\rm S}\hat{D} - \frac{1}{2}\{\rho_{\rm S},\hat{D}\hat{D}^\dagger\}\Big) + \Gamma_{\rm r}\cos^2\alpha\,[1-f_{\rm r}(\varepsilon_D)]\Big(\hat{D}\rho_{\rm S}\hat{D}^\dagger - \frac{1}{2}\{\rho_{\rm S},\hat{D}^\dagger\hat{D}\}\Big)\\ & + \Gamma_{\rm r}\sin^2\alpha\, f_{\rm r}(\varepsilon_d)\Big(\hat{d}^\dagger\rho_{\rm S}\hat{d} - \frac{1}{2}\{\rho_{\rm S},\hat{d}\hat{d}^\dagger\}\Big) + \Gamma_{\rm r}\sin^2\alpha\,[1-f_{\rm r}(\varepsilon_d)]\Big(\hat{d}\rho_{\rm S}\hat{d}^\dagger - \frac{1}{2}\{\rho_{\rm S},\hat{d}^\dagger\hat{d}\}\Big)\\ & + \text{cross terms proportional to } \sin\alpha\cos\alpha,\end{aligned} \tag{B3}$$

analogous to left lead, without counting fields for energy/particle as needed.

$$\begin{aligned}\mathcal{L}_{\rm ph}[\rho_{\rm S}] \;=\; & \cos^2(2\alpha)\,\Gamma_{\rm ph}N_q\left({\rm e}^{+{\rm i}\lambda_{\rm ph}\omega_0}\hat{D}^\dagger\hat{d}\rho_{\rm S}\hat{d}^\dagger\hat{D} - \frac{1}{2}\{\rho_{\rm S},\hat{d}^\dagger\hat{D}\hat{D}^\dagger\hat{d}\}\right)\\ & + \cos^2(2\alpha)\,\Gamma_{\rm ph}\,(N_q+1)\left({\rm e}^{-{\rm i}\lambda_{\rm ph}\omega_0}\hat{d}^\dagger\hat{D}\rho_{\rm S}\hat{D}^\dagger\hat{d} - \frac{1}{2}\{\rho_{\rm S},\hat{D}^\dagger\hat{d}\hat{d}^\dagger\hat{D}\}\right)\\ & - \cos^2(2\alpha)\Gamma_{\rm ph}M_q\hat{D}^\dagger\hat{d}\rho_{\rm S}\hat{D}^\dagger\hat{d} - \cos^2(2\alpha)\Gamma_{\rm ph}M_q^*\hat{d}^\dagger\hat{D}\rho_{\rm S}\hat{d}^\dagger\hat{D}\\ & + \text{additional terms proportional to } \sin(2\alpha)\cos(2\alpha),\end{aligned} \tag{B4}$$

accounting for squeezing-induced correlations between $\hat{D}$ and $\hat{d}$.

Here, the hybridization energies are defined as

$$\begin{aligned}\Gamma_v(\varepsilon) &= 2\pi\sum_k |\gamma_{kv}|^2\delta(\varepsilon-\varepsilon_k), \quad v=\mathrm{l},\mathrm{r},\\ \Gamma_{\mathrm{ph}}(\omega) &= 2\pi\sum_q |\gamma_{\mathrm{e\text{-}ph}}|^2\delta(\omega-\omega_q),\end{aligned} \tag{B5}$$

under the wide-band approximation. The electronic Fermi functions are

$$f_v(\varepsilon) = \frac{1}{\exp[(\varepsilon-\mu_v)/k_{\mathrm{B}}T_v]+1}, \tag{B6}$$

while the photonic occupation and squeezing parameters are

$$\begin{aligned}N_q &= \left(n_{\mathrm{ph}}+\frac{1}{2}\right)\cosh(2r)-\frac{1}{2},\\ M_q &= \left(n_{\mathrm{ph}}+\frac{1}{2}\right)\mathrm{e}^{\mathrm{i}\theta}\sinh(2r),\\ n_{\mathrm{ph}}(\omega_0) &= \frac{1}{\exp(\beta_{\mathrm{ph}}\omega_0)-1}, \qquad \omega_0=\varepsilon_D-\varepsilon_d.\end{aligned} \tag{B7}$$

Appendix C: Vectorization of the quantum master equation

To numerically solve the χ-resolved quantum master equation and derive the Liouvillian matrix $\boldsymbol{L}(\chi)$, we employ the *vectorization* technique. This method transforms the operator-valued master equation for the density matrix ρ_{S} into a matrix-vector equation for the vectorized density matrix $|\boldsymbol{P}(\chi,t)\rangle$. We define the vectorization map vec, which maps an operator X to a column vector $|X\rangle$ (often denoted as $\boldsymbol{X}$ in the literature). The fundamental property of this map is that for any three operators A, X, and B of compatible dimensions

$$\mathrm{vec}(AXB) = (B^{\mathsf{T}}\otimes A)\cdot\mathrm{vec}(X),$$

where $\otimes$ denotes the Kronecker product and B^{T} is the transpose of B. In quantum mechanics, we frequently deal with Hermitian operators. If B is Hermitian ($B^\dagger = B$), then $B^{\mathsf{T}} = B^*$ (complex conjugate). A more practical form for our purpose is

$$\mathrm{vec}(A\rho B) = (B^\dagger\otimes A)|\rho\rangle, \tag{C1}$$

where $|\rho\rangle\equiv\mathrm{vec}(\rho)$ is the column vector obtained by stacking the columns of the density matrix ρ. The master equation contains not only terms like $A\rho B$ but also anticommutators of the form $\{\rho,X\}=\rho X+X\rho$. Using the map rule in Eq. (C1), we can derive

$$\begin{aligned}\mathrm{vec}(\rho X) &= (X^{\mathsf{T}}\otimes I)|\rho\rangle,\\ \mathrm{vec}(X\rho) &= (I\otimes X)|\rho\rangle.\end{aligned}$$

Therefore, the vectorization of the anticommutator $\{\rho,X\}$ is given by

$$\mathrm{vec}(\{\rho,X\}) = \left[(X^{\mathsf{T}}\otimes I)+(I\otimes X)\right]|\rho\rangle.$$

If X is a Hermitian operator ($X^\dagger = X$), it follows that $X^{\mathsf{T}} = X^*$. Consequently, the vectorized form of the anticommutator is given by

$$\mathrm{vec}(\{\rho,X\}) = \left[(X^*\otimes I)+(I\otimes X)\right]|\rho\rangle. \tag{C2}$$

This form is standard in the derivation of Lindblad-type dissipators.

The right-hand side of the master equation (Eq. (B1)) comprises a sum of terms, each being a linear combination of the forms $A\rho B$ or $\{\rho,X\}$. Our objective is to recast the entire differential equation,

$$\frac{\mathrm{d}\rho_{\mathrm{S}}(\chi,t)}{\mathrm{d}t} = \mathcal{L}(\chi)[\rho_{\mathrm{S}}(\chi,t)],$$

into a linear system for the vectorized density matrix

$$\frac{\mathrm{d}|\boldsymbol{P}(\chi,t)\rangle}{\mathrm{d}t} = \boldsymbol{L}(\chi)|\boldsymbol{P}(\chi,t)\rangle,$$

where $|\boldsymbol{P}(\chi,t)\rangle = \mathrm{vec}(\rho_{\mathrm{S}}(\chi,t))$, and $\boldsymbol{L}(\chi)$ is the matrix representation of the Liouvillian superoperator $\mathcal{L}(\chi)$ in the vectorized space.

Applying the vectorization rules (Eqs. (C1) and (C2)) to each term in the master equation, we obtain the explicit contributions to the total Liouvillian matrix $\boldsymbol{L}(\chi)$ from the left electronic reservoir. For brevity, the coupling strength Γ_{l} is factored out in the expressions below:

$$L_1 = \Gamma_{\mathrm{l}}\sin^2(\alpha)f_{\mathrm{l}}(\varepsilon_D)\left(\mathrm{e}^{+\mathrm{i}\lambda_{\mathrm{p}}+\mathrm{i}\lambda_E\varepsilon_D}\hat{D}^{\mathsf{T}}\otimes\hat{D}^{\mathsf{T}}-\frac{1}{2}\hat{D}\hat{D}^{\mathsf{T}}\otimes\mathrm{I}-\frac{1}{2}\mathrm{I}\otimes\hat{D}\hat{D}^{\mathsf{T}}\right),$$

$$L_2 = \Gamma_{\mathrm{l}}\sin^2(\alpha)[1-f_{\mathrm{l}}(\varepsilon_D)]\left(\mathrm{e}^{-\mathrm{i}\lambda_{\mathrm{p}}-\mathrm{i}\lambda_E\varepsilon_D}\hat{D}\otimes\hat{D}-\frac{1}{2}\hat{D}^{\mathsf{T}}\hat{D}\otimes\mathrm{I}-\frac{1}{2}\mathrm{I}\otimes\hat{D}^{\mathsf{T}}\hat{D}\right),$$

$$L_3 = \Gamma_{\mathrm{l}}\cos^2(\alpha)f_{\mathrm{l}}(\varepsilon_d)\left(\mathrm{e}^{+\mathrm{i}\lambda_{\mathrm{p}}+\mathrm{i}\lambda_E\varepsilon_d}\hat{d}^{\mathsf{T}}\otimes\hat{d}^{\mathsf{T}}-\frac{1}{2}\hat{d}\hat{d}^{\mathsf{T}}\otimes\mathrm{I}-\frac{1}{2}\mathrm{I}\otimes\hat{d}\hat{d}^{\mathsf{T}}\right),$$

$$L_4 = \Gamma_{\mathrm{l}}\cos^2(\alpha)[1-f_{\mathrm{l}}(\varepsilon_d)]\left(\mathrm{e}^{-\mathrm{i}\lambda_{\mathrm{p}}-\mathrm{i}\lambda_E\varepsilon_d}\hat{d}\otimes\hat{d}-\frac{1}{2}\hat{d}^{\mathsf{T}}\hat{d}\otimes\mathrm{I}-\frac{1}{2}\mathrm{I}\otimes\hat{d}^{\mathsf{T}}\hat{d}\right),$$

$$
\begin{aligned}
L_5 &= -\frac{1}{2}\Gamma_{\rm l}\sin\alpha\cos\alpha\left(\mathrm{e}^{\mathrm{i}\lambda_{\rm p}+\mathrm{i}\lambda_E\varepsilon_D}f_{\rm l}(\varepsilon_D)+\mathrm{e}^{\mathrm{i}\lambda_{\rm p}+\mathrm{i}\lambda_E\varepsilon_d}f_{\rm l}(\varepsilon_d)\right)(\hat{D}^{\mathsf{T}}\otimes\hat{d}^{\mathsf{T}}+\hat{d}^{\mathsf{T}}\otimes\hat{D}^{\mathsf{T}}),\\
L_6 &= -\frac{1}{2}\Gamma_{\rm l}\sin\alpha\cos\alpha\left(\mathrm{e}^{\mathrm{i}\lambda_{\rm p}+\mathrm{i}\lambda_E\varepsilon_D}(1-f_{\rm l}(\varepsilon_D))+\mathrm{e}^{\mathrm{i}\lambda_{\rm p}+\mathrm{i}\lambda_E\varepsilon_d}(1-f_{\rm l}(\varepsilon_d))\right)(\hat{D}\otimes\hat{d}+\hat{d}\otimes\hat{D}),\\
L_7 &= -\frac{1}{2}\Gamma_{\rm l}\sin\alpha\cos\alpha(f_{\rm l}(\varepsilon_D)+f_{\rm l}(\varepsilon_d)-1)\left(\hat{d}^{\mathsf{T}}\hat{D}\otimes\mathrm{I}+\hat{D}^{\mathsf{T}}\hat{d}\otimes\mathrm{I}+\mathrm{I}\otimes\hat{D}^{\mathsf{T}}\hat{d}+\mathrm{I}\otimes\hat{d}^{\mathsf{T}}\hat{D}\right),
\end{aligned}
\tag{C3}
$$

The corresponding contributions from the right electronic reservoir, denoted as R_i, can be obtained by substituting $\alpha\to\alpha-\pi/2$ into the expressions for L_i.

Following the same vectorization procedure, we now derive the contributions from the squeezed photon reservoir to the total Liouvillian matrix $\boldsymbol{L}(\chi)$. The terms associated with the photon reservoir, as given in the master equation (Eq. (B1)), are more complex due to the inelastic electron–photon interaction and the non-classical nature of the squeezed reservoir. Nevertheless, they can be systematically decomposed into the fundamental forms of $A\rho B$ and $\{\rho,X\}$, allowing us to apply the same vectorization rules.

The contributions from the photon reservoir, denoted as L_8 to L_{19}, are enumerated below:

$$
\begin{aligned}
L_8 &= \cos^2(2\alpha)\Gamma_{\rm ph}N_q\left(\mathrm{e}^{+\mathrm{i}\lambda_{\rm ph}\omega_0}(\hat{d}^\dagger\hat{D})^{\mathsf{T}}\otimes(\hat{D}^\dagger\hat{d})^{\mathsf{T}}-\frac{1}{2}\left[\mathrm{I}\otimes(\hat{d}^\dagger\hat{D}\hat{D}^\dagger\hat{d})+((\hat{d}^\dagger\hat{D}\hat{D}^\dagger\hat{d})^{\mathsf{T}}\otimes\mathrm{I})\right]\right),\\
L_9 &= \cos^2(2\alpha)\Gamma_{\rm ph}(N_q+1)\left(\mathrm{e}^{-\mathrm{i}\lambda_{\rm ph}\omega_0}(\hat{D}^\dagger\hat{d})^{\mathsf{T}}\otimes(\hat{d}^\dagger\hat{D})^{\mathsf{T}}-\frac{1}{2}\left[\mathrm{I}\otimes(\hat{D}^\dagger\hat{d}\hat{d}^\dagger\hat{D})+((\hat{D}^\dagger\hat{d}\hat{d}^\dagger\hat{D})^{\mathsf{T}}\otimes\mathrm{I})\right]\right),\\
L_{10} &= -\cos^2(2\alpha)\Gamma_{\rm ph}M_q\left((\hat{D}^\dagger\hat{d})^{\mathsf{T}}\otimes(\hat{D}^\dagger\hat{d})^{\mathsf{T}}\right),\\
L_{11} &= -\cos^2(2\alpha)\Gamma_{\rm ph}M_q^*\left((\hat{d}^\dagger\hat{D})^{\mathsf{T}}\otimes(\hat{d}^\dagger\hat{D})^{\mathsf{T}}\right),\\
L_{12} &= +\frac{1}{2}\Gamma_{\rm ph}\sin(2\alpha)\cos(2\alpha)N_q\left(\mathrm{I}\otimes(\hat{D}^\dagger\hat{d}\hat{D}^\dagger\hat{D})+((\hat{D}^\dagger\hat{d}\hat{D}^\dagger\hat{D})^{\mathsf{T}}\otimes\mathrm{I})\right),\\
L_{13} &= -\frac{1}{2}\Gamma_{\rm ph}\sin(2\alpha)\cos(2\alpha)((N_q+1)-\mathrm{e}^{-\mathrm{i}\lambda_{\rm ph}\omega_0}M_q^*)\left(\mathrm{I}\otimes(\hat{d}^\dagger\hat{D}\hat{d}^\dagger\hat{d})+((\hat{d}^\dagger\hat{D}\hat{d}^\dagger\hat{d})^{\mathsf{T}}\otimes\mathrm{I})\right),\\
L_{14} &= -\frac{1}{2}\Gamma_{\rm ph}\sin(2\alpha)\cos(2\alpha)(N_q+1)\left((\hat{d}^\dagger\hat{d})^{\mathsf{T}}\otimes(\hat{D}^\dagger\hat{d})^{\mathsf{T}}+(\hat{D}^\dagger\hat{d})^{\mathsf{T}}\otimes(\hat{d}^\dagger\hat{d})^{\mathsf{T}}\right),\\
L_{15} &= +\frac{1}{2}\Gamma_{\rm ph}\sin(2\alpha)\cos(2\alpha)N_q\left((\hat{D}^\dagger\hat{D})^{\mathsf{T}}\otimes(\hat{d}^\dagger\hat{D})^{\mathsf{T}}+(\hat{d}^\dagger\hat{D})^{\mathsf{T}}\otimes(\hat{D}^\dagger\hat{D})^{\mathsf{T}}\right),\\
L_{16} &= -\frac{1}{2}\Gamma_{\rm ph}\sin(2\alpha)\cos(2\alpha)\mathrm{e}^{+\mathrm{i}\lambda_{\rm ph}\omega_0}N_q\left((\hat{D}^\dagger\hat{D})^{\mathsf{T}}\otimes(\hat{D}^\dagger\hat{d})^{\mathsf{T}}-(\hat{d}^\dagger\hat{d})^{\mathsf{T}}\otimes(\hat{D}^\dagger\hat{d})^{\mathsf{T}}\right),\\
L_{17} &= +\frac{1}{2}\Gamma_{\rm ph}\sin(2\alpha)\cos(2\alpha)\mathrm{e}^{-\mathrm{i}\lambda_{\rm ph}\omega_0}(N_q+1)\left((\hat{D}^\dagger\hat{D})^{\mathsf{T}}\otimes(\hat{d}^\dagger\hat{D})^{\mathsf{T}}-(\hat{d}^\dagger\hat{d})^{\mathsf{T}}\otimes(\hat{d}^\dagger\hat{D})^{\mathsf{T}}\right),\\
L_{18} &= -\frac{1}{2}\Gamma_{\rm ph}\sin(2\alpha)\cos(2\alpha)\mathrm{e}^{-\mathrm{i}\lambda_{\rm ph}\omega_0}(N_q+1)\left((\hat{D}^\dagger\hat{d})^{\mathsf{T}}\otimes(\hat{D}^\dagger\hat{D})^{\mathsf{T}}-(\hat{D}^\dagger\hat{d})^{\mathsf{T}}\otimes(\hat{d}^\dagger\hat{d})^{\mathsf{T}}\right),\\
L_{19} &= +\frac{1}{2}\Gamma_{\rm ph}\sin(2\alpha)\cos(2\alpha)\mathrm{e}^{+\mathrm{i}\lambda_{\rm ph}\omega_0}N_q\left((\hat{d}^\dagger\hat{D})^{\mathsf{T}}\otimes(\hat{D}^\dagger\hat{D})^{\mathsf{T}}-(\hat{d}^\dagger\hat{D})^{\mathsf{T}}\otimes(\hat{d}^\dagger\hat{d})^{\mathsf{T}}\right).
\end{aligned}
\tag{C4}
$$

The terms L_8 and L_9 represent standard dissipative processes involving single-photon exchange, dressed by the coherent coupling between the dots. The terms L_{10} and L_{11}, proportional to M_q and M_q^*, are unique to the squeezed reservoir and originate from two-photon correlations. The remaining terms (L_{12}–L_{19}) describe more intricate dissipative channels that arise from the interplay between the squeezed bath and the coherent superpositions within the DQD system, which are crucial for generating the steady-state coherence and entanglement discussed in the main text.

For numerical implementation in the full four-state basis $\{|0\rangle,|d\rangle,|D\rangle,|dD\rangle\}$, the electronic operators have matrix representations

$$
\hat{d}=\begin{pmatrix}0&1&0&0\\0&0&0&0\\0&0&0&1\\0&0&0&0\end{pmatrix},\quad \hat{D}=\begin{pmatrix}0&0&1&0\\0&0&0&-1\\0&0&0&0\\0&0&0&0\end{pmatrix},
$$

while the diagonalized DQD Hamiltonian is $\hat{H}_{\rm DQD}=\mathrm{diag}(0,\varepsilon_d,\varepsilon_D,\varepsilon_d+\varepsilon_D)$.

With the contributions from the left electronic reservoir (Eq. (C3)), the photon reservoir (Eq. (C4)), and the right electronic reservoir obtained via the substitution $\alpha\to\alpha-\pi/2$, the construction of the full Liouvillian superoperator $\boldsymbol{L}(\chi)$ is complete. This matrix encapsulates the entire dynamics of

the three-terminal DQD system, including the effects of the squeezed reservoir and the counting fields, and serves as the foundation for all subsequent calculations of transport quantities and quantum correlations presented in this work.

Acknowledgments

Project supported by the National Natural Science Foundation of China (Grant Nos. 12305050 and 52302298) and the Natural Science Foundation of Jiangsu Higher Education Institutions of China (Grant No. 23KJB140017).

References

[1] Benenti G, Casati G, Saito K and Whitney R S 2017 *Phys. Rep.* **694** 1
[2] Wang R, Wang C, Lu J and Jiang J H 2022 *Adv. Phys. X* **7** 2082317
[3] Jiang J H, Entin-Wohlman O and Imry Y 2012 *Phys. Rev. B* **85** 075412
[4] Jiang J H and Imry Y 2017 *Phys. Rev. Appl.* **7** 064001
[5] Liu H, Wang C, Wang L Q and Ren J 2019 *Phys. Rev. E* **99** 032114
[6] Lu J, Wang R, Wang C and Jiang J H 2023 *Entropy* **25** 498
[7] Bu K, Singh U, Fei S M, Pati A K and Wu J 2017 *Phys. Rev. Lett.* **119** 150405
[8] Camati P A, Santos J F G and Serra R M 2019 *Phys. Rev. A* **99** 062103
[9] Engel G S, Calhoun T R, Read E L, Ahn T K, Mančal T, Cheng Y C, Blankenship R E and Fleming G R 2007 *Nature* **446** 782
[10] Sánchez R, Gorini C and Fleury G 2021 *Phys. Rev. B* **104** 115430
[11] Sánchez R, Splettstoesser J and Whitney R S 2019 *Phys. Rev. Lett.* **123** 216801
[12] Roßnagel J, Abah O, Schmidt-Kaler F, Singer K and Lutz E 2014 *Phys. Rev. Lett.* **112** 030602
[13] Klaers J, Faelt S, Imamoglu A and Togan E 2017 *Phys. Rev. X* **7** 031044
[14] Niedenzu W, Mukherjee V, Ghosh A, Kofman A G and Kurizki G 2018 *Nat. Commun.* **9** 165
[15] Xiao Y, Liu D, He J, Zhuang L, Liu W M, Yan L L and Wang J 2023 *Phys. Rev. Res.* **5** 043185
[16] Lê T K, Lukin D M, Roques-Carmes C, Karnieli A, Lustig E, Guidry M A, Fan S and Vučković J 2024 arXiv:2412.15068 [quant-ph]
[17] Cao B, Han C, Hao X, Wang C and Lu J 2024 *Chin. Phys. Lett.* **41** 077302
[18] Landi G T and Paternostro M 2021 *Rev. Mod. Phys.* **93** 035008
[19] Bhandari B and Jordan A N 2022 *Phys. Rev. Res.* **4** 033103
[20] Esposito M, Harbola U and Mukamel S 2009 *Rev. Mod. Phys.* **81** 1665
[21] Landi G T, Kewming M J, Mitchison M T and Potts P P 2024 *PRX Quantum* **5** 020201
[22] Agarwalla B K, Jiang J H and Segal D 2015 *Phys. Rev. B* **92** 245418
[23] Lu J, Liu J, Jiang J H and Wang C 2025 *Phys. Rev. B* **111** 245407
[24] Yamamoto K and Hatano N 2015 *Phys. Rev. E* **92** 042165
[25] Lu J, Jiang J H and Imry Y 2021 *Phys. Rev. B* **103** 085429
[26] Jiang J H, Kulkarni M, Segal D and Imry Y 2015 *Phys. Rev. B* **92** 045309
[27] Lu J, Wang Z, Ren J, Wang C and Jiang J H 2024 *Phys. Rev. B* **109** 125407
[28] Cao B, Han C, Hao X, Wang C and Lu J 2024 *Chin. Phys. Lett.* **41** 077302
[29] Zhang L, Wang J S and Li B 2010 *Phys. Rev. B* **81** 100301
[30] Ren J and Zhu J X 2013 *Phys. Rev. B* **88** 094427
[31] Yang Y, Chen H, Wang H, Li N and Zhang L 2018 *Phys. Rev. E* **98** 042131
[32] Zhang Y and Su S 2021 *Physica A* **584** 126347
[33] Wang C, Xu D, Liu H and Gao X 2019 *Phys. Rev. E* **99** 042102
[34] Díaz I and Sánchez R 2021 *New J. Phys.* **23** 125006
[35] Tesser L, Bhandari B, Erdman P A, Paladino E, Fazio R and Taddei F 2022 *New J. Phys.* **24** 035001
[36] Khandelwal S, Perarnau-Llobet M, Seah S, Brunner N and Haack G 2023 *Phys. Rev. Res.* **5** 013129
[37] Lu J, Wang R, Ren J, Kulkarni M and Jiang J H 2019 *Phys. Rev. B* **99** 035129
[38] Li B, Wang L and Casati G 2006 *Appl. Phys. Lett.* **88** 143501
[39] Li N, Ren J, Wang L, Zhang G, Hänggi P and Li B 2012 *Rev. Mod. Phys.* **84** 1045
[40] Lu J, Wang R, Wang C and Jiang J H 2020 *Phys. Rev. B* **102** 125405
[41] Bergenfeldt C, Samuelsson P, Sothmann B, Flindt C and Büttiker M 2014 *Phys. Rev. Lett.* **112** 076803
[42] Sánchez R, Thierschmann H and Molenkamp L W 2017 *Phys. Rev. B* **95** 241401
[43] Yang Y, Zhao Y and Zhang L 2023 *Appl. Phys. Lett.* **122** 232201
[44] Guo B Q, Liu T and Yu C S 2018 *Phys. Rev. E* **98** 022118
[45] Wang C, Chen X M, Sun K W and Ren J 2018 *Phys. Rev. A* **97** 052112